Abstract. The exchanges of carbon, water, and energy between the atmosphere and the Amazon Basin have global implications for current and future climate. Here, the global atmospheric inversion system of the Monitoring of Atmospheric Composition and Climate service (MACC) is used to study the seasonal and interannual variations of biogenic CO_2 fluxes in Amazonia during the period 2002–2010. The system assimilated surface measurements of atmospheric CO_2 mole fractions made at more than 100 sites over the globe into an atmospheric transport model. The present study adds measurements from four surface stations located in tropical South America, a region poorly covered by CO_2 observations. The estimates of net ecosystem exchange (NEE) optimized by the inversion are compared to an independent estimate of NEE upscaled from eddy-covariance flux measurements in Amazonia. They are also qualitatively evaluated against reports on the seasonal and interannual variations of the land sink in South America from the scientific literature. We attempt at assessing the impact on NEE of the strong droughts in 2005 and 2010 (due to severe and longer-than-usual dry seasons), and of the extreme rainfall conditions registered in 2009. The spatial variations of the seasonal and interannual variability of optimized NEE are also investigated. While the inversion supports the assumption of strong spatial heterogeneity of these variations, the results reveal critical limitations of coarse resolution transport model, of the surface observation network in South America during the recent years, and of the present knowledge of modelling uncertainties in South America that prevent our inversion from capturing the seasonal patterns of fluxes across Amazonia. However, some patterns from the inversion seem consistent with the anomaly of moisture conditions in 2009.

1 Introduction

The forests of Amazonia cover $6.77\,\mathrm{million\,km^2}$ (INPE, 2011). It is the world's largest continuous area of tropical forest and reservoir of aboveground organic carbon (Malhi et al., 2008). Changes in the carbon dynamics of this ecosystem thus have global significance (Wang et al., 2013). However, the natural variability of $\mathrm{CO_2}$ exchange in Amazonia, as well as its short and long term response to natural and anthropogenic disturbance across scales, is still poorly understood and a topic of active research.

There is intense debate about the timing and magnitude of the seasonal cycle of $\mathrm{CO_2}$ fluxes across Amazonia. Studies employing remote sensing data as a proxy for canopy photosynthetic activity have suggested a widespread enhancement of gross primary productivity (GPP) of the Amazonian rainforest during the dry season (Huete et al., 2006). Yet, direct and continuous measurements of net ecosystem exchange (NEE) between the atmosphere and forest canopy at a local scale (from $1\,\mathrm{ha}$ to $1\,\mathrm{km^2}$ scale) based on eddy-covariance (EC) systems do not support such large-scale behaviour. Several EC observations in central eastern Amazonia (Saleska et al., 2003) and northeastern Amazonia (Bonal et al., 2008) also indicate that tropical forest areas take up $\mathrm{CO_2}$ during the dry season, but similar EC studies in central Amazonia have suggested an opposite seasonality (Grace et al., 1996; Araújo et al., 2002). Finally, remote sensing measurements of the vertically integrated columns of $\mathrm{CO_2}$ ($\mathrm{XCO_2}$) retrieved from the GOSAT satellite, suggest stronger $\mathrm{CO_2}$ uptake during the wet season in southern Amazonian forest than during the dry season (Parazoo et al., 2013). These measurements thus reveal a large heterogeneity in space of the phase of the seasonal cycle of NEE within Amazonia. However, most dynamic global vegetation model (DGVM) simulations predict stronger uptake during the wet season throughout Amazonia (Verbeeck et al., 2011; Saleska et al., 2003; Baker et al., 2008; Poulter et al., 2009), although limitations related to mortality or land use restrict the ability of these generic global models to simulate $\mathrm{CO_2}$ fluxes and carbon stocks of Amazonian forest (Gloor et al., 2012).

Uncertainty associated with potential spatial heterogeneity is also apparent in the estimates of the interannual variability (IAV) of $\mathrm{CO_2}$ fluxes in Amazonia, in particular during years with extreme climatic conditions. Remote sensing observations during the severe Amazonian drought of 2005 suggested a widespread enhancement of photosynthetic activity, or greening, across Amazonia

(Saleska et al., 2007). The resilience of forests to water stress suggested by the "drier-yet-greener" papers was originally attributed to a combination of deep rooting, hydraulic redistribution, and more available solar radiation (Saleska et al., 2007). However, the validity of enhanced vegetation index (EVI) satellite data has been recently challenged by Morton et al. (2014) and by losses in canopy functioning detected in radar-based measurements (Saatchi et al., 2012). The observations from optical satellite sensors remain controversial because other studies did not find such an impact of droughts on Amazonian forest (Xu et al., 2011; Samanta et al., 2010, 2012). Moreover, observations of microwave backscatter from QuickSCAT have suggested large-scale, persistent negative effects of the drought of 2005 on forest canopy structure (Saatchi et al., 2012). Biometry measurements, consisting of periodic measurements of the allocation of photosynthetic products to wood growth, provide another perspective on the effects of drought on Amazonian forest trees. In a large-scale, long-term biometric study, Phillips et al. (2009) found a reversal of the carbon sink due to the effect of the drought of 2005 on tree mortality. This is consistent with a synthesis of yearly estimates of natural fluxes (NEE plus biomass-burning emissions) from an ensemble of DGVMs compiled at http://www.globalcarbonatlas.org.

The scientific community has used atmospheric inversions for more than two decades in an effort to improve the knowledge of CO_2 fluxes at large scale. Whereas EC or biometric studies give flux estimates that are valid at local scale (Ometto et al., 2005), atmospheric inversion offers the possibility to derive measurement-based estimates for the whole of Amazonia, with spatial resolutions larger than 500 km, provided that atmospheric observations can adequately sample the Amazonian flux signal. Inversions use available measurements of atmospheric CO_2 to provide corrections to prior surface flux estimates using an atmospheric transport model and statistical inversion methods. The method estimates statistically optimal fluxes within the boundaries of uncertainties in the measurements, the transport model, and prior flux estimates (Enting et al., 1995; Ciais et al., 2010). The flux corrections spread beyond the vicinity of the measurement footprint, as defined by the transport model, through hypotheses on the spatial and temporal correlation of the uncertainties in the prior fluxes. We define, hereafter, the tropical South America (TSA) region as the continental land encompassed between 16.25° N–31.25° S and 84.38° W–28.18° W, which covers the whole Amazonian forest. Peylin et al. (2013) show that the different inverted seasonal cycles and IAVs of natural CO_2 fluxes from several state-of-the-art global atmospheric inversions are characterized by a large scatter over a very similar tropical area of South America. This is explained by the variety of prior estimates used by the different global inversion systems, and by the large-scale corrections that are applied in regions poorly covered by observation networks, such as TSA, in order to balance the global CO_2 budget, rather than to match local measurements. For these reasons, atmospheric inversions have not been included in the review of the carbon cycle in South America made by Gloor et al. (2012). Lloyd et al. (2007) and Gatti et al. (2010) applied the principle of atmospheric inversion to exploit vertical CO_2 profiles data from airborne measurements in Amazonia. Their studies, based on measurements near Manaus, in central Amazonia (Lloyd et al., 2007), and Santarém in eastern Amazonia (Gatti et al., 2010), constitute important efforts to constrain surface CO_2 fluxes at regional scale, measuring and exploiting some of the few atmospheric data sets available for South America. Their results suggested CO_2 efflux from the ecosystem during the wet season in eastern Amazonia. By analysing vertical CO_2 profiles collected approximately every two weeks over the period 2010–2011, the recent study of Gatti et al. (2014) provided a basin-scale picture that confirms this regional signal, but that also suggests an opposite pattern in southern and western Amazonia. Their study reported on the first data-driven estimate of CO_2 fluxes for the whole Amazon basin and it provides insight into the sensitivity of this important ecosystem to moisture stress. It suggests the importance of conducting such estimates over longer time periods.

Our goal here is to study the seasonal cycle and IAV of NEE over Amazonia during 2002–2010. This period offers the opportunity to investigate significant anomalies in the interannual variability of carbon fluxes, particularly those associated with the severe droughts of 2005 and 2010, and with the extreme rainfall registered across the Amazon basin in 2009 (Marengo et al., 2010). The study is based on the global MACC inversion system initially described by Chevallier et al. (2010) (hereafter

CH2010). We used version 10.1 of the MACC CO_2 inversion product released in August 2011. We also use a similar inversion in which we add four ground-based atmospheric measurement sites surrounding the northeast of Amazonia to the assimilated data (Fig. 1). Despite the limitations of the state-of-the-art global inversion approach in South America, highlighted above and by Gloor et al. (2012), our analysis of these MACC inversions can help characterizing the temporal variations in the NEE over Amazonia for several reasons. First, it relies on a detailed evaluation of the inversion results over and within this region, hoping that some reliable inversion patterns can be isolated. Such a detailed evaluation has not been conducted in the above-mentioned inter-comparisons of the global atmospheric inversions in TSA. It makes sense to conduct it here on the MACC inversions since the MACC system uses a variational inversion which solves for the fluxes at $\sim 3^{\circ}$and 8-day spatial and temporal resolution. Second, the use of the stations located in the region can strengthen the robustness of the inversion results through a significantly increased sampling of the atmospheric signature of the fluxes in Amazonia. In particular, we are the first to use continuous measurements from French Guyana. The assessment of the impact of these stations on the inverted NEE (based on the comparison between our different MACC inversions with and without these stations) can help identify the reliable patterns of the inversion.

The rest of this paper is structured as follows. We present each component of the standard MACCv10.1 inversion setup and the use of the additional sites around Amazonia in Sect. 2. The results of the inversions, with a focus on the impact of these additional sites, and their comparison to an independent flux estimate are presented in Sect. 3. In Sect. 4, we discuss the results and conclude the study.

2 The inversion method

This study builds on MACC the global atmospheric inversion framework (whose first version is described in detail in CH2010) to correct a prior estimate of NEE from the model ORCHIDEE (Organizing Carbon and Hydrology in Dynamic Ecosystems, Krinner et al., 2005) and of ocean fluxes, based on the assimilation of in situ measurements of atmospheric CO_2 mole fractions into a global atmospheric transport model. The approach relies on a Bayesian framework to estimate the conditional probability of the "true" NEE and ocean fluxes given the statistical information from the prior fluxes and the set of in situ measurements of atmospheric CO_2 (hereafter *observations*). Assumption of unbiased Gaussian distribution of the uncertainties in the prior fluxes and of those underlying the simulation of the observations using the transport model, allows us to derive an updated estimate of NEE and ocean fluxes (hereafter the posterior fluxes) that also has an unbiased Gaussian distribution. The statistically optimal fluxes (i.e., the mean of the posterior distribution of the fluxes) are found by calculating the minimum of the cost function (Tarantola, 2005)

$$J(\boldsymbol{x}) = (\boldsymbol{x} - \boldsymbol{x}^{\mathrm{b}})^{\mathrm{T}} \mathbf{B}^{-1} (\boldsymbol{x} - \boldsymbol{x}^{\mathrm{b}}) + (\boldsymbol{y}^{\mathrm{o}} - H(\boldsymbol{x}))^{\mathrm{T}} \mathbf{R}^{-1} (\boldsymbol{y}^{\mathrm{o}} - H(\boldsymbol{x})) \quad (1)$$

where $\boldsymbol{x}$ is the control vector and mainly denotes the NEE (defined as the difference between the gross CO_2 uptake through photosynthesis and output through total ecosystem respiration), and air–ocean exchanges that are optimized at a chosen spatial and temporal resolution. $\boldsymbol{x}^{\mathrm{b}}$ represents the prior NEE and ocean fluxes, and $\boldsymbol{y}^{\mathrm{o}}$ is the vector of observations. H is the operator projecting $\boldsymbol{x}$ into the observation space, and is based on an atmospheric transport model and fossil fuel and biomass-burning CO_2 emission estimates.

$\mathbf{B}$ and $\mathbf{R}$ are the covariance matrices of the normal distribution of the uncertainty in $\boldsymbol{x}^{\mathrm{b}}$ (the "prior uncertainty") and of the sum in the observation space of the other uncertainties when comparing $H(\boldsymbol{x}^{\mathrm{b}})$ to $\boldsymbol{y}^{\mathrm{o}}$, respectively (the "observation errors"). The latter includes the measurement, model transport and model representation errors. A complete solution to the inversion problem requires the estimation of the uncertainty in the optimized fluxes (the "posterior uncertainty"), which is a function of the prior and of the observation errors. As explained below in Sect. 2.1, this estimation was not performed in this study. The following sections present a brief description of each component of the

inversion configuration used in this study with a focus on parameters that are specific to this study, while CH2010 provides more details on the parameters which apply to all the MACC inversion configurations.

2.1 Inversion modelling setup

The link between CO_2 fluxes and observations in the MACC inversion is simulated by the global circulation model of the Laboratoire de Météorologie Dynamique (LMDZ) (version 4, Hourdin et al., 2006), which is the atmospheric component of the coupled climate model of the Institut Pierre Simon Laplace IPSL-CM4. Tracer transport is simulated by LMDZ at a horizontal resolution of $3.75° \times 2.75°$ (longitude $\times$ latitude) and with a vertical resolution of 19 levels between the surface and the top of the atmosphere. LMDZ is nudged to winds modelled by the European Centre for Medium-Range Weather Forecasts (ECMWF). Prior NEE in MACCv10.1 was estimated at $3.75° \times 2.75°$ and 3 h resolution from a global simulation of the ORCHIDEE model at 0.7° resolution by Maignan et al. (2011). ORCHIDEE was forced with the atmospheric conditions of ECMWF reanalysis ERA-Interim (Berrisford et al., 2009). The ORCHIDEE NEE did not take into account disturbance from land use or wildfires. Prior ocean–atmosphere CO_2 exchanges were obtained from the climatology of air–ocean CO_2 partial pressure difference by Takahashi et al. (2009).

To complement these fluxes that were controlled by the inversion, the H operator also included fixed estimates of the fossil fuel and biomass-burning CO_2 emissions. Fossil fuel emissions were obtained from the EDGAR-3.2 Fast Track 2000 database (Olivier and Berdowski, 2001), scaled annually with the global totals of the Carbon Dioxide Information Analysis Center (CDIAC). CO_2 emissions from biomass burning were taken from the Global Fires Emission Database version 2 (GFEDv2, Randerson et al., 2007). Assuming that the vegetation recovers rapidly from fire events, the CO_2 emissions from fires that affected the vegetation in a given year were offset by an equivalent compensatory regrowth CO_2 uptake evenly distributed throughout the year.

The inversion controlled 8-day mean daytime and nighttime NEE and 8-day mean ocean fluxes at the spatial resolution of the transport model. The analysis in this study focuses on NEE, thus the impact of the inversion on ocean fluxes is not detailed here, but Sect. 3.2 still uses an illustration of this impact to raise insights into the corrections from the inversion over land. At the grid scale, uncertainties in the prior NEE are estimated to be proportional to the heterotrophic respiration fluxes from ORCHIDEE. Spatial correlations of the uncertainties in $\mathbf{B}$ decay exponentially as a function of the distance between corresponding pixel-based estimates of the fluxes with a length scale of 500 km for NEE (1000 km for ocean fluxes). Temporal correlations of the uncertainties decay exponentially as a function of the lag-time between the corresponding 8-day mean daytime or nighttime estimate of the fluxes with a timescale of one month, but without correlation between daytime and nighttime uncertainties. The resulting correlations in $\mathbf{B}$ are estimated as the product between the temporal and the spatial correlations. This setup of the correlations for $\mathbf{B}$ is based on the estimates by Chevallier et al. (2006) and Chevallier et al. (2012) of differences between the NEE simulated by ORCHIDEE and EC flux measurements (mostly located in the Northern Hemisphere).

In the inversion framework, the misfits between simulated CO_2 mole fractions and the measurements that are not due to uncertainty in the prior NEE or ocean fluxes must be accounted for in the covariance matrix $\mathbf{R}$. Uncertainties in fire and anthropogenic CO_2 emissions are assumed to have negligible impact at the measurement locations used here. Therefore, they are ignored in the setup of $\mathbf{R}$. Following CH2010, the measurement errors are assumed to be negligible in comparison to the uncertainties in the transport model. Model transport and representation errors are modelled as half the variance of the high frequency variability of the deseasonalized and detrended CO_2 time series of the measurements that are assimilated at a given station. The resulting values of these model errors for the stations in South America will be discussed in Sect. 3.1.

There is a moderate confidence in the adequacy of these error statistics assigned in the global inversion system for the specific TSA area studied here, both because $\mathbf{B}$ was designed mostly with statistics gathered in the Northern Hemisphere, and because $\mathbf{R}$ may not well account for the uncer-

tainty in the atmospheric convection model, while this could be high in Amazonia (Parazoo et al., 2008). We also investigate here variations of the fluxes within TSA at spatial scales that are not much larger than the e-folding correlation length in $\mathbf{B}$, and these variations in the inversion results may be affected by our simple hypothesis of isotropic correlations in the prior uncertainty. This lack of confidence in the input error statistics weakens our confidence in the posterior error statistics that can be derived based on the inversion system, even though they may be realistic at zonal scale for the Tropics (Chevallier and O'Dell, 2013). In this context, and given the relatively high computational burden of the posterior uncertainty computations for grid-point inversion systems (using Monte Carlo approaches with ensembles of inversions, Chevallier et al., 2007), we do not derive these posterior uncertainties for our domain and its sub-domains.

However, we will see at the beginning of Sect. 3 that the inverted fluxes are more consistent with the CO_2 atmospheric observations in TSA than the prior fluxes, and that their difference to the prior fluxes over TSA (i.e. the flux increments generated by the inversion in order to better fit with the observations) are significant. This indicates that the inverted fluxes are strongly driven by the atmospheric data and as such, are worth analysing. This also suggests that the inversions yield a large uncertainty reduction for TSA.

2.2 Assimilated data

MACCv10.1 assimilated measurements of atmospheric CO_2, expressed as dry air mole fractions in $\mu\mathrm{mol\,mol^{-1}}$ (abbreviated ppm), from 128 surface sites: 35 continuous measurement stations and 93 sites with measurements of CO_2 from discrete air samples collected approximately weekly. 29 sites are located in the tropics, but only two had continuous measurements over the analysis period and none of them were in TSA. In a similar inversion conducted specifically for this study, called INVSAm hereafter, we added new data from four surface sites located in the TSA region. Figure 1 shows the measurement sites used by MACCv10.1 and the four stations added in INVSAm. In the following of this section, we focus on the description of these four stations and on the selection and representation of their data. Details on the data selection and representation at the sites used by MACCv10.1 are provided in CH2010.

Arembepe (ABP) (12.77° S, 38.17° W, 1 masl) and Maxaranguape (MAX) (5.51° S, 35.26° W, 15 masl) are coastal stations. The ABP site is located at the edge of the beach, where vegetation consists mostly of grass and beach plants. Data were collected at approximately $8\,\mathrm{m}$ above the ground, and consisted of weekly measurements of atmospheric CO_2 with discrete air samples, specifically under on-shore wind conditions, when wind speed $> 2\,\mathrm{m\,s^{-1}}$. Air samples were collected preferentially during the afternoon to avoid the influence of recycled air transported from land to the ocean by land breeze during the night and early morning, and transported back to land by sea-breeze during the morning. The MAX site is located on a cliff right next to the coast, and is surrounded by grass and beach plants. At MAX, CO_2 was measured with a continuous analyzer, at approximately $3\,\mathrm{m}$ above the ground, and data were reported as 30 min averages. This site is strongly under marine influence: winds are in general $> 10\,\mathrm{m\,s^{-1}}$, and wind direction varies preferentially between 100°and 140°(Kirchhoff et al., 2003) at its location, so that the measurements were taken mostly under on-shore wind conditions. Wind and CO_2 measurements at MAX indicate high CO_2 variations when the wind comes from land. These variations may be strongly influenced by the emissions from the nearby city of Maxaranguape (Kirchhoff et al., 2003). However, as in ABP, this does not occur during the afternoon, when the wind conditions are dominated by sea-breeze (Law et al., 2010).

The Guyaflux site (GUY) (5.28° N, 52.91° W, 40 masl) is located at approximately 11 km from the coast, and is surrounded by undisturbed tropical forest. At GUY, measurements were taken at approximately 55 m above the ground (Bonal et al., 2008). They were made with a continuous analyser, and data were reported as hourly averages. The Santarém site (SAN) (2.85° S, 54.95° W, 78 masl) is located in the tropical Tapajós National Forest, near km 67 of the Santarém–Cuiabá highway, at approximately 750 km from the coast. Measurements were made at 8 vertical levels ranging from

$\sim$1 to $\sim$62 m above the ground with continuous analyzers, but only data from the highest level were used in INVSAm. Data were reported as hourly averages.

Figure 2 illustrates the temporal coverage of the observations available in TSA during the simulated period (2002–2010). There is little overlap among the site records, due to calibration problems, interruption of the measurements (e.g., at MAX) and the fact that some stations have been installed only recently (e.g., at GUY). The longest records were from ABP (3 years: 2007–2009) and SAN (4 years: 2002–2005). Data from the four new sites in TSA have been calibrated on the WMO-X2007 CO_2 scale, managed by the ESRL/NOAA.

Prevailing winds in the lower troposphere across TSA convey air masses entering from the Atlantic Ocean near the Equator across the continent and back into the southern Atlantic Ocean generally south of 20° S. There are no critical seasonal variations of the mean winds in the area so that this typical behaviour applies throughout the year. The climatology of wind fields from the NCEP/NCAR reanalysis (over the period 1981–2010) for February, July and annual mean, shown in Fig. 3, illustrates this typical circulation pattern. This confirms that the variations of CO_2 at coastal stations (ABP, MAX) are mainly influenced by air–ocean exchanges and fluxes in distant lands. These stations should thus provide more information on the atmospheric CO_2 content upwind of TSA, than on the fluxes within Amazonia. Fig. 3 also shows that GUY and SAN receive a signal from the ecosystems of the northeastern Amazon Basin. Despite GUY being not far from the coast considering the Amazon-wide scale, this site is still located inland, in an area covered by undisturbed, tropical wet forest. SAN is located considerably further inland than GUY. Typical influence functions of fluxes for observations at GUY and SAN (the observation "footprints", in Fig. 3b and c, respectively) illustrate that the sensitivity of instantaneous mole fractions to the fluxes rapidly decreases with the distance mainly due to the typically moderate horizontal wind speeds, so that they should bear a strong signature of local fluxes i.e., of the NEE in northeastern Amazonia. This, and the fact that the geographical distance between the sites in the TSA region ranges from 1000 to 2600 km, i.e. up to five times the correlation length scale in the matrix $\mathbf{B}$, could suggest that the area well constrained by the sites in the TSA region through inversion is limited. However, as illustrated in Fig. 3, the station footprints also have modest values over very extensive areas which may also result in significant large-scale constraint from the inversion on the land flux estimates. This will be analyzed below in Sect. 3.2.

We assimilated observations from the South American sites between 12:00 and 15:00 local time (LT), when the boundary layer (BL) is well developed and likely to be well represented by the transport model (Butler et al., 2010; Gatti et al., 2010). Such a selection of the afternoon data results in ignoring the measurements under off-shore flow at MAX, and thus the potential for capturing a clear signature of the regional NEE at this site such as at ABP. However, this potential is rather low since under off-shore flow conditions the signal at MAX is also connected to the local anthropogenic emissions, and the inversion cannot reliably exploit such a signature of the regional NEE when the dynamics of the PBL are poorly represented by the atmospheric transport model. Observations were also screened for low wind speed ($> 2\,\mathrm{m\,s^{-1}}$), thus removing the effect of local emissions (and sinks) that may not be well captured by the transport model at resolution $3.75° \times 2.5°$. Under such on-shore flow conditions, the model correctly simulates CO_2 in the grid-cells corresponding to the horizontal location of the coastal sites, even though these grid-cells bear a significant NEE due to the overlapping of both land and ocean. This reduces the need for ad hoc changes of the model grid-cells to better represent CO_2 at the coastal sites (e.g., Law et al., 2010). In a general way, we choose to represent the four measurements sites using the model horizontal grid-cell in which they are located since, for each site, it yields better statistical fit between the prior simulations and the selected measurements than when using neighbour grid-cells.

2.3 Analysis of an alternative estimate of the NEE for the evaluation of the inversions

Our analysis of the inversion results is compared to the independently derived NEE estimated by Jung et al. (2011) (hereafter J2011). J2011 used model tree ensembles (MTE), a machine-learning

technique, to upscale FLUXNET eddy-covariance observations, based on remote sensing, climate, and land-use data as drivers, thereby producing gridded estimates of NEE and other surface fluxes at the global scale at 0.5°resolution. As discussed in J2011, large uncertainties affect their annual mean NEE estimates and associated seasonal and interannual variations. This is likely particularly true in TSA region, where few FLUXNET measurements are available. Yet, its comparison to the NEE from the inversion could give useful insights for the analysis of the latter.

3 Results

In this section we first analyze the statistical misfits between observations and simulated mole fractions from prior and posterior fluxes at the sites in the TSA area, as a measure of the efficiency of the inversion in reducing the misfits to the measurements. This is a first indicator of the significance of the corrections applied to the fluxes. We then examine the amplitude and spatial distribution of the increments from both inversions to give a further indicator of this significance, and to characterize the impact of assimilating the measurements from the sites in South America. Finally we focus on the impact of the inversions on the seasonal patterns and IAV of NEE which are the aim of this study. This analysis is supported by the comparison to the product of J2011.

3.1 Comparison to observed CO_2 mole fractions

The time series of assimilated observations and the corresponding simulated CO_2 mole fractions using the prior fluxes, the inverted fluxes from MACCv10.1 and that from INVSAm at the four sites in the TSA region are plotted in Fig. 4. The statistics of the misfits between these measured and simulated CO_2 mole fractions are summarized in Fig. 5. At each site in the TSA region, the smallest quadratic mean and standard deviation of the misfits between the simulations and the observations were obtained with INVSAm, which is a logical consequence of the assimilation of these observations. However, the misfits are also strongly decreased at all sites when comparing MACCv10.1 to the prior simulation. While, compared to the prior simulation, MACCv10.1 strongly decreases the standard deviation of the misfits at MAX and APB, it does not significantly reduce it at GUY and SAN. The decrease of the misfits at all sites in MACCv10.1 is thus explained by the strong decrease of the bias in these misfits. Indeed, both inversions critically reduce a large-scale bias over TSA, since the presence of a few marine stations on the globe is enough to introduce this effect by correcting the global growth rate of CO_2 (CH2010). However, the information from the local network significantly impacted the seasonality of the simulated CO_2 in the TSA region.

The resulting optimized mole fractions from INVSAm generally shifted from a minimum to a maximum around June every year at SAN or from a maximum to a minimum around October (both in 2004 and 2006) at MAX with respect to the prior simulation and MACCv10.1 (Fig. 4c) and in agreement with the observations. While yielding a phase of seasonality at GUY comparable to that of the prior simulation and MACCv10.1, and comparable to that of the data, INVSAm exhibits a significant rescaling of the seasonal variations in the period from May to September at this site (Fig. 4b) compared to these two other simulations, in agreement with the observations. At SAN, during the austral fall-winter, while the misfits are negative with MACCv10.1, they become positive with INVSAm. The positive increments from the assimilation of data at SAN (no other data are assimilated in TSA in 2002 and 2003) are thus too high.

Subsequently, when compared to MACCv10.1, INVSAm improves the amplitude of the seasonal variations of the simulated mole fractions with respect to the prior simulation at GUY and MAX and does not impact it at SAN. At ABP, the seasonality is less visible in both the measurements and the inversion posterior simulations and it is difficult to assess whether INVSAm improves it compared to MACCv10.1, but both inversions dramatically decrease the large amplitude of the prior seasonal variations, consistent with the data. The best correlations with the observations are obtained with INVSAm at all sites (Fig. 5). The values of these correlations remained generally low, ranging from 0.23 at GUY to 0.81 at ABP. These correlations are based on comparison of daily CO_2 mole

fractions while the inversions control 8-day mean fluxes, which strongly limits the ability to impact the mole fractions at higher temporal resolution, and which can thus explain the low correlation values. Correlations between time series of observed and simulated monthly mean mole fractions are higher than those for daily values, ranging from 0.76 at GUY to 0.92 at ABP for INVSAm, with which, again, these correlations are the highest.

The significance of the reduction of the misfits between the mole fractions observed and simulated from the inversion is seen from the comparison between the standard deviations of these misfits and the estimate of the standard deviation of the observation errors (i.e. of the transport model errors) for hourly values in the configuration of the $\mathbf{R}$ matrix (Table A1, in supplementary material). According to this comparison, the prior misfits are much larger than the observation errors at ABP, MAX, and GUY, but are slightly smaller than these at SAN. Misfits between MACCv10.1 and the observations are similar to the prior misfits at SAN and GUY and are much smaller than the prior misfits (and smaller than the 95% confidence interval of the observations) at the coastal ABP and MAX sites. Misfits are further decreased when assimilating the data from the South American sites: they are about the standard deviation of the observation errors at all sites but GUY (where they are twice as large).

These results suggest that the assimilation of data in the TSA region helped improve the phasing of the seasonal variations, whereas MACCv10.1 did not impact it. MACCv10.1 mainly improved the amplitude of the seasonal variations at the coastal sites and decreased the biases. INVSAm improved the amplitude of the seasonal variations at GUY. More generally, unlike MACCv10.1, INVSAm led to an improvement of the variability of the simulated CO_2 at the inland sites, which are more sensitive to the NEE in Amazonia.

3.2 Characterization of the monthly to annual mean inversion increments to the prior fluxes

Figure 6 shows the spatial distribution of the mean corrections applied during the period 2002–2010 by INVSAm and MACCv10.1 over land and ocean, across an area that covers the TSA area and neighbour regions. In complement, Fig. S1 shows the spatial distribution of the corrections over land in the TSA region for the full 2002–2010 period, and for the 2002–2005 and 2006–2010 sub-periods. Both give results for the full years and for the months of February and July. As such, these figures are indicative of the amplitude and spatial extent of the corrections from the inversions, and of the impact of the assimilation of the measurements in South America. Figure S1 even dissociates the impact of assimilating data at SAN and MAX and that of assimilating data at MAX, ABP and GUY by splitting the results between the time periods when these two different sets of data are available. The analysis of the annual mean corrections and of mean corrections for February and July should also give first insights on the significance of the corrections applied to the seasonal cycle and IAV of the NEE in the TSA region.

Figure 6 depicts the increments from both inversions, showing large patterns which are nearly zonal (or along the prevailing winds) and which overlap continuously over land and ocean. Since there is no correlation between the uncertainty in ocean and land fluxes in the $\mathbf{B}$ matrix, and given the typical length scale of the correlations in this matrix, this can be directly connected to the signature of atmospheric transport. The contiguous zonal patterns have alternate negative and positive flux increments. There is thus an opposition between corrections in the North and in the South of the TSA region. These corrections are rather negative in the North and positive in the South (positive in the North and negative in the South) during the austral summer (winter). As these corrections are stronger during the austral winter, it results in positive (negative) corrections in the North (South) at the annual scale. Such dipoles are a typical behaviour of inverse modelling systems in data-poor regions (Peylin et al., 2002). However, changes in the amplitude and latitudinal position of this zonal dipole appear to be the main impact from the assimilation of data in the TSA region. This dipole structure may thus yield sensible corrections to the NEE in the TSA area. The dipole has a high amplitude for MACCv10.1, and even higher for INVSAm. The increments from INVSAm to the annual fluxes often exceed 150% of the prior estimate in terms of absolute values. The highest

increments are obtained during austral winter and when the SAN data are available (during the period 2002–2005, see Fig. S1), which is in line with the fact that this site is located more inland than the others. Such high control of the data in the TSA region (even when checking the SAN and MAX, or the MAX, ABP and GUY datasets only) over the zonal patterns of flux corrections also highlights the very large-extent impact of these data, and of the data in the southern hemisphere in general, despite the relatively small spatial correlation length scales in the $\mathbf{B}$ matrix, and the limited area in which the station footprints are very high. The inversion also generates patterns of corrections of smaller spatial scale close to the measurement sites in the TSA region when these sites are used by the inversion. This raises hope that the NEE over the whole TSA region is strongly constrained by the observations, but can also raise questions regarding the spatial variations of the corrections applied by the inversion to the NEE within the TSA region, at least when considering areas at more than 500 km from the measurement sites. However, various pieces of evidence (Fig. 5 and 6, the analysis of the decrease in misfits to the observations from the inversion in Sect. 3.1, and the previous analysis of the high increments to the monthly mean and annual mean NEE over the entire TSA region) indicate that the corrections from the inversion are significant.

3.3 Diagnostics of the biogenic CO_2 fluxes

3.3.1 Seasonality

Figure 7a illustrates the mean seasonal cycle of NEE from the prior fluxes, J2011, MACCv10.1 and INVSAm over TSA. The mean for the full period 2002–2010 was removed because uncertainties in the long-term mean can be large for the inversions as well as for the J2011 product, and because this long-term mean can differ significantly between the different estimates. Removing the mean allows us to focus on the seasonal variations. Hereafter, positive values of NEE indicate anomalous CO_2 release to the atmosphere; negative values indicate anomalous uptake by the ecosystems. The shaded area indicates the dry season, defined as months with precipitation $< 100\,\mathrm{mm}$ according to data from the Tropical Rainfall Measuring Mission (TRMM 3B43 (v6) product), averaged over January 2002 to June 2010. The results of Fig. 7a are calculated considering all the plant functional types (PFTs) represented in ORCHIDEE over the TSA region. The vegetation map of ORCHIDEE, originally at a spatial resolution of 0.72°, was aggregated according to the transport model grid, and Fig. 8 illustrates the dominant PFTs in terms of area for each transport model grid-cell.

Both the prior simulation and the inversions predict a maximum of NEE (i.e., likely a maximum of CO_2 release) in the dry season and a minimum of NEE (i.e., likely a maximum of CO_2 uptake) in the wet season (Fig. 7a). This behaviour is also seen in J2011. However, J2011 places the maximum of NEE during the transition between the wet and dry season while the prior simulation and the inversions place it at the end of the dry season. Even though the inversions seem to delay or lengthen this maximum, such a modification is not significant and their seasonal phasing is likely strongly constrained by the patterns of the prior fluxes. In particular, according to the comparison between INVSAm and MACCv10.1, the assimilation of data from the four stations in the TSA region does not seem to impact this phasing.

The inland data are prone to bear a stronger signature from fluxes in tropical broadleaf evergreen and raingreen (TBE) forests (Fig. 8), while the mean seasonal behaviour over the whole TSA region could be mainly related to other PFTs. Therefore, we isolate the results for the area of TBE forests, this area being defined by the selection the model grid-cells dominated by this vegetation type. The configuration of the prior uncertainties in the inversion does not account for PFTs, so that the spread of the flux corrections in the inversions is not forced a priori to depend on vegetation type. We still expect that the variations in the measurements, when their footprint covers different distributions of PFTs, reflect differences in NEE of the PFTs. Consequently, the spatial patterns of the increments from the inversion may be consistent with the spatial patterns of NEE induced by the distribution of the different vegetation types. The mean seasonal cycle of NEE for the area of TBE forests within the TSA region is given in Fig. 7b. The restriction of the analysis to the TBE forest does not show

any clear correlation between NEE extremes and the phasing of wet and dry seasons, neither when considering the NEE from the prior nor when considering the NEE from both inversion estimates. This is different from J2011 that indicates a maximum of the NEE a few months before the beginning of the dry season and a minimum of the NEE at the beginning of the wet season. The prior and the inversions indicate several local extremes of NEE throughout the year that may reflect the overlapping of significantly different seasonal cycles for different sub-regions within TBE forests.

The strong spatial heterogeneity of the time variations of the NEE in TBE forests has been discussed in the introduction. Fig. S2 illustrates it this with results of local NEE mean seasonal cycle estimated from EC measurements across TSA. This figure also shows the mean seasonal cycle of the precipitation at these sites to illustrate the spatial heterogeneity of the drivers of NEE within TSA.

To examine whether the inversion captures this spatial variability of the fluxes, we analyze the seasonal variations of the NEE estimates for the two zones depicted in Fig. 8. Zone 1 was located in northeastern Amazonia, close to the measurement stations SAN and GUY. Zone 2 was located in central eastern Amazonia. Both zones are mainly covered by TBE forests, according to the vegetation classification of ORCHIDEE. According to Malhi et al. (2009), eastern Amazonia is drier, and shows a stronger seasonality than western Amazonia. However, we do not identify a clear pattern of NEE seasonal variations that could be driven by the rainfall seasonality in any of the two sub-regions, except for J2011 in Zone 1 (Fig. 7c), since the other estimates again exhibited maxima and minima of NEE during both dry and wet seasons. Actually, in Zone 2 (Fig. 7d) the dry season cannot not be clearly identified. In this zone, the prior flux and the inversions indicated several maxima and minima of NEE, but J2011 exhibite, again, a clear seasonal cycle with a maximum in June and a minimum October as in Zone 1. While J2011 showed nearly the same amplitude and phasing of monthly mean NEE variations in both zones and over TBE forests (Fig. 7b), prior and inversions estimates of the seasonal variations differed both in phasing and amplitude between zone 1, 2 and the whole TBE forest area.

Divergent patterns are found in INVSAm with respect to MACCv10.1, which remains closer to the prior fluxes, even though the departure of MACCv10.1 from the prior NEE is significant in Zone 2 and for the whole TBE area (Fig. 7b and 7d). The comparison of these inversion results shows that significant flux corrections due to the assimilation of data in South America are applied in Zone 1 (Fig. 7c), i.e., in northeastern Amazonia, where stations SAN and GUY are located. The influence of SAN over this zone is clearer when splitting the analysis period of the mean seasonal cycles between 2002–2005 and 2006–2010 (not shown). The differences between INVSAm and MACCv10.1 are more accentuated during the period 2002–2005, when SAN is active. However, there are still significant changes between these two estimates during 2006–2010. The changes between MACCv10.1 and INVSAm in Zone 2 (Fig. 7d) are also significant, even though Zone 2 seems hardly observed by the TSA observation network. As analysed in Sect. 3.2, the control of the long-range dipole (of its amplitude and latitudinal position) by the measurements in region TSA explains such an impact of these measurements on the results in Zone 2, as well as that of measurements outside South America, which explains the departure of MACCv10.1 from the prior NEE in zone 2. Zone 2 is actually located close to the frontier between the Northern and Southern patterns of the dipole in the TSA region. A latitudinal shift of the frontier through the assimilation of data in northeastern Amazonia can thus easily imply that positive (negative) increments from the inversion are reverted into negative (positive) increments.

In an attempt at getting clearer seasonal patterns in some of the other sub-regions of Amazonia, two additional zones have been analyzed, located in southwestern and southeastern Amazonia, where the dry season is potentially earlier and more extreme (Fig. S2a,d). Both sub-regions encompass areas where the impact of the droughts of 2005 and 2010 was the highest according to Lewis et al. (2011). The results, however, do not provide any further information than Fig. 7c,d and are not shown. J2011 still exhibit the same amplitude of the seasonal cycle and the same location of maximum and minimum NEE as in zones 1 and 2 despite the extent of the dry season. Prior fluxes and inversions still showed maxima and minima during the dry season in some cases, and the inversions introduce only slight modifications to the amplitude and phasing of the NEE relative to the

prior simulation. This is an expected result due to insufficient data in the southern part of the TSA to constrain fluxes in that region.

3.3.2 Interannual variability

Figure 9a depicts the annual NEE anomalies of the prior simulation, MACCv10.1, INVSAm and an additional inversion called FLAT, compared to their mean NEE over 2002–2010, aggregated over the whole TSA region (considering all PFTs). FLAT corresponds to a new inversion using, as a prior estimate, a "flat prior" whose annual anomalies are null over the TSA region. Using the standard prior NEE as a basis, the flat prior is built by offsetting the annual budgets of NEE over the TSA region so that they equal the mean annual NEE over TSA and over the 2002–2010 period from the standard prior NEE. The spatial variability and the temporal variability at scales smaller than a year are conserved between the standard NEE and the flat prior, since the offsets are applied homogeneously in space and time within TSA and within one year. FLAT assimilates the data from the four surface sites in TSA in addition to those used by both MACCv10.1 and INVSAm. Of note is that even if increments on the NEE annual budget of a given year from an inversion are weak, the changes in the corresponding annual anomaly from the inversion can be high because the inversion modifies the 2002–2010 average against which the anomaly is computed. Prior fluxes, MACCv10.1 and INVSAm display only small positive anomalies during the drought years (2005, 2010) compared to other years. FLAT displays a negative anomaly (i.e., a strong uptake) in 2010, but it indicates a larger positive anomaly in 2005 than that of other estimates. On the other hand, the strong NEE negative anomaly of 2009 in the prior fluxes, MACCv10.1 and INVSAm is also in FLAT, which suggests that this pattern is strongly driven by the atmospheric measurements, and which raises confidence in it.

As in Sect. 3.3.1, we isolated the results for the TBE forests area (Fig. 9b). In this case, prior fluxes and both MACCv10.1 and INVSAm estimates show diverging annual mean responses of forests to drought, with a positive anomaly in 2005 and a negative anomaly in 2010. For 2009, when climatic conditions were abnormally humid across South America, the inversion estimates consistently show a small positive anomaly, opposite to the response for the whole TSA region. The small anomalies in all inversions suggest a weak sensitivity of the NEE of TBE forests to interannual variations and that most of the IAV over the study area is not related to TBE forests.

Finally, we analyze the results in the two sub-regions shown in Fig. 8, in an attempt to identify potential differences in the regional responses. NEE estimates from the prior, INVSAm and MACCv10.1 show various responses of forests to drought in these zones. In zone 1 (Fig. 10a) all these estimates present a positive anomaly in 2005 and a negative anomaly in 2010, while in zone 2 (Fig. 10b) they yielded negative anomalies during both years. J2011 exhibit abnormal anomalies much smaller than these NEE estimates (Fig. 10c and d). This prevents us from getting insights into the IAV from the comparison of J2011 to the other estimates. However, the product of J2011 must be used cautiously, especially when evaluating IAV of NEE. J2011 relied on a limited number of EC stations across the Amazon basin, with short time series, to estimate MTE based on spatial gradients among the sites, and then extrapolated to temporal gradients. This is valid assuming that spatial and temporal NEE patterns have the same sensitivity to climate, which may be incorrect (Piao et al., 2013). The example of the divergences of the results between MACCv10.1 and INVSAm in 2003 in Zone 2 illustrates, again, some weak ability to precisely constrain the fluxes in such a small area, which is quite distant from the measurement sites in TSA. Indeed, the analysis of the maps of increments from MACCv10.1 and INVSAm for the annual mean NEE in 2003 (not shown) demonstrates that the assimilation of data at SAN during this year shifts the northern border of the pattern of negative corrections in MACCv10.1 from North of Zone 2 to the south of Zone 2. Since, on average, over 2002–2010, both inversions apply positive increments in this Zone (see Fig. 6) this leads to a clear negative annual anomaly in Zone 2 and for the year 2003 for INVSAm.

4 Discussion and concluding remarks

Amazonian forests play a key role in the global carbon balance, but there are large uncertainties on the evolution of this terrestrial sink. Uncertainties stem from incomplete knowledge of the processes behind land–atmosphere CO_2 exchange in this region. Improving our understanding of the seasonal and interannual variations of Amazonian forests is thus a priority. In an attempt to gain insight into how these temporal variations of CO_2 fluxes vary across Amazonia, we analysed global inversions and incorporated new measurements of atmospheric CO_2 mole fractions in TSA into one of these inversions. The analysis of the global inversions at such spatial scales, which are generally ignored in global inversion studies, is justified by the use of a variational inversion system solving for the fluxes at $\sim 3^{\circ}$and 8-day resolution. We showed that the two inversions applied large corrections to the estimates of NEE from a vegetation model that they used as prior information. The inverted NEE was strongly controlled by the assimilation of CO_2 measurements both outside and within the TSA region, and this control was characterized by zonal patterns of alternate positive and negative corrections, which we call "zonal dipole", in addition to more local patterns in the vicinity of the sites that were assimilated.

Despite an overall improvement by the inversion of the seasonal variations of the simulated CO_2 mole fractions when compared to the measurements in TSA, several issues arose when analyzing the seasonal cycles of NEE from the inversion. The seasonality of the mean NEE over the whole TSA region remained basically unchanged between the inversion estimates (Fig. 7a). The prior and inversion estimates of this mean seasonal cycle of NEE at the TSA scale are not in line with J2011 and disagree with the intuitive assumption that the seasonal cycle should be correlated with rainfall and solar radiation, especially in the tropical forest area. Furthermore, they do not exhibit a clear seasonal pattern over TBE forests at basin scale or within the analyzed sub-regions. J2011 displays a clear, homogeneous seasonal cycle all the TSA region, which does not give confidence in its ability to distinguish regional heterogeneity. The proximity of Zone 1 to the stations in northeastern Amazonia (SAN and GUY) (Fig. 8) suggests better confidence in the flux corrections applied by INVSAm to the prior fluxes in that zone than elsewhere in TSA region.

The reliability in the seasonal patterns of the inverted fluxes is thus not high, which seems to confirm that the zonal dipoles of increments from the inversion are artificial patterns, which balance the overall correction in the Southern Hemisphere, and which are not necessarily consistent with the actual NEE in the TSA region. This is directly connected to the lack of CO_2 measurements in the TSA region, both in space and time. The limited overlap among the TSA observations is a critical issue since measurements are often only available at a single site at once, and consequently, temporary model errors at this site can get far more weight in the inversion than if it had been balanced by information from other sites. Furthermore, the lack of confidence in the INVSAm results in Zone 1, which is relatively close to the GUY and SAN, suggests a low reliability in the statistics of the uncertainty in the prior NEE (in the inversion configuration), on which the extrapolation of the information from the vicinity of these sites to the whole North East of the TSA region relies. This further supports the choice of avoiding computing posterior uncertainties in the inverted NEE as discussed in Sect. 2.1.

Such considerations also weaken the analysis of the IAV based on the inversion while J2011 does not provide a reliable IAV of the NEE in TSA, which could have supported such an analysis. But some patterns of the IAV in the NEE seem consistent between the different inversion estimates when the atmospheric measurements have a strong control on it: across the TSA region, the estimates from the prior fluxes, MACCv10.1, INVSAm and FLAT indicate small positive flux annual anomalies (CO_2 release) during the drought in 2005 and a strong negative (CO_2 sink) anomaly in 2009, presumably related to lower temperatures and more humid conditions in 2009. However, in 2010 there is a divergence of the results between the FLAT estimate and the others.

In the TBE forests, the highest source anomaly in 2005 seen in the prior fluxes, MACCv10.1 and INVSAm may be related to reduced photosynthesis during the drought, as found by Gatti et al. (2014), and/or tree mortality caused by the squall event of January 2005 (Negrón-Juárez et al., 2010).

However, in 2010 these results indicate a small sink anomaly. This anomaly seems inconsistent with the hypothesis of a higher negative impact of the drought in 2010, which was more intense in terms of water stress and more geographically extensive (Lewis et al., 2011). On the other hand, it seems consistent with the recent results of Gatti et al. (2014), who found that the Amazon basin was carbon neutral during that year.

Even though some seasonal or interannual patterns from the inversion look realistic, our study mainly reveals some critical issues that hamper the ability to derive an accurate estimation of the temporal variability of NEE and of its spatial heterogeneity across Amazonian forests. A denser monitoring network across the basin with continuous time series, as initiated by Gatti et al. (2014), is needed to well constrain the fluxes in the region. In addition, the simulation of atmospheric transport may need to be handled with models that are better adapted to the local meteorological conditions. Regional transport models with higher spatial and temporal resolution and improved parameterizations of key atmospheric processes for the region (e.g., deep convection, Parazoo et al., 2008) have been developed (Moreira et al., 2013). The combination of a denser observation network and state-of-the-art regional modelling tools would overcome some of the critical limitations encountered here for the study of the temporal variability of biosphere CO_2 fluxes in Amazonia. Such regional inversion will require reliable regional configurations of the input error statistics, which could rely on extensions of the flux eddy covariance measurement networks in Amazonia. Finally, adaptive strategies for the representation of the observations in the model simulations as a function of the sites and of the meteorological conditions (Law et al., 2010) could help loosen the selection of the data for the assimilation.

Acknowledgements. We would like to thank Martin Jung (Max Planck Institute for Biogeochemistry) for the access to the upscaled NEE data. Data recorded at the GUY site were obtained in the framework of the GUYAFLUX project funded by the French Ministry of Research, INRA, and the CNES, in the framework of the PO Feder Région Guyane. The GUYAFLUX project also received support from an Investissement d'Avenir grant of the French ANR (CEBA: ANR-10-LABX-0025). This study was co-funded by the European Commission under the EU Seventh Research Framework Programme (grant agreement No. 283080, Geocarbon project) and ARIA Technologies. G. Broquet acknowledges funding and support from the Chaire industrielle BridGES, a joint research program between Thales Alenia Space, Veolia, CEA, UVSQ and CNRS.

References

Araújo, A. C., Nobre, A. D., Kruijt, B., Elbers, J. A., Dallarosa, R., Stefani, P., von Randow, C., Manzi, A. O., Culf, A. D., Gash, J. H. C., Valentini, R., and Kabat, P.: Comparative measurements of carbon dioxide fluxes from two nearby towers in a central Amazonian rainforest: the Manaus LBA site, J. Geophys. Res., 107, 8090, doi:10.1029/2001JD000676, 2002.

Baker, I. T., Prihodko, L., Denning, A. S., Goulden, M., Miller, S., and da Rocha, H. R.: Seasonal drought stress in the Amazon: reconciling models and observations, J. Geophys. Res., 113, G00B01, doi:10.1029/2007JG000644, 2008.

Berrisford, P., Dee, D., Fielding, K., Fuentes, M., Kallberg, P., Kobayashi, S., and Uppala, S.: The ERA-Interim archive, Tech. rep., European Centre for Medium Range Weather Forecasts, Reading, 2009.

Bonal, D., Bosc, A., Ponton, S., Goret, J.-Y., Burban, B., Gross, P., Bonnefond, J.-M., Elbers, J., Longdoz, B., Epron, D., Guehl, J.-M., and Granier, A.: Impact of severe dry season on net ecosystem exchange in the neotropical rainforest of French Guiana, Glob. Change Biol., 14, 1917–1933, doi:10.1111/j.1365-2486.2008.01610.x, 2008.

Borma, L. S., da Rocha, H. R., Cabral, O. M., von Randow, C., Collicchio, E., Kurzatkowski, D., Brugger, P. J., Freitas, H., Tannus, R., Oliveira, L., Rennó, C. D., and Artaxo, P.: Atmosphere and hydrological controls of the evapotranspiration over a floodplain forest in the Bananal Island region, Amazonia, J. Geophys. Res., 114, G01003, doi:10.1029/2007JG000641, 2009.

Butler, M. P., Davis, K. J., Denning, A. S., and Kawa, S. R.: Using continental observations in global atmospheric inversions of CO_2: North American carbon sources and sinks, Tellus B, 62, 550–572, doi:10.1111/j.1600-0889.2010.00501.x, 2010.

Carswell, F. E., Costa, A. L., Palheta, M., Malhi, Y., Meir, P., Costa, J. d. P. R., Ruivo, M. d. L., Leal, L. d. S. M., Costa, J. M. N., Clement, R. J., and Grace, J.: Seasonality in CO_2 and H_2O flux at an eastern Amazonian rain forest, J. Geophys. Res., 107, LBA 43-1–LBA 43-16, doi:10.1029/2000JD000284, 2002.

Chevallier, F. and O'Dell, C. W.: Error statistics of Bayesian CO_2 flux inversion schemes as seen from GOSAT, Geophys. Res. Lett., 40, 1252–1256, doi:10.1002/grl.50228, 2013.

Chevallier, F., Viovy, N., Reichstein, M., and Ciais, P.: On the assignment of prior errors in Bayesian inversions of CO_2 surface fluxes, Geophys. Res. Lett., 33, L13802, doi:10.1029/2006GL026496, 2006.

Chevallier, F., Bréon, F.-M., and Rayner, P. J.: Contribution of the Orbiting Carbon Observatory to the estimation of CO_2 sources and sinks: Theoretical study in a variational data assimilation framework, J. Geophys. Res., 112, n/a–n/a, doi:10.1029/2006JD007375, 2007.

Chevallier, F., Ciais, P., Conway, T. J., Aalto, T., Anderson, B. E., Bousquet, P., Brunke, E. G., Ciattaglia, L., Esaki, Y., Fröhlich, M., Gomez, A., Gomez-Pelaez, A. J., Haszpra, L., Krummel, P. B., Langenfelds, R. L., Leuenberger, M., Machida, T., Maignan, F., Matsueda, H., Morguí, J. A., Mukai, H., Nakazawa, T., Peylin, P., Ramonet, M., Rivier, L., Sawa, Y., Schmidt, M., Steele, L. P., Vay, S. A., Vermeulen, A. T., Wofsy, S., and Worthy, D.: CO_2 surface fluxes at grid point scale estimated from a global 21 year reanalysis of atmospheric measurements, J. Geophys. Res., 115, D21307, doi:10.1029/2010JD013887, 2010.

Chevallier, F., Wang, T., Ciais, P., Maignan, F., Bocquet, M., Altaf Arain, M., Cescatti, A., Chen, J., Dolman, A. J., Law, B. E., Margolis, H. A., Montagnani, L., and Moors, E. J.: What eddy-covariance measurements tell us about prior land flux errors in CO_2-flux inversion schemes, Global Biogeochem. Cycles, 26, n/a–n/a, doi:10.1029/2010GB003974, 2012.

Ciais, P., Rayner, P., Chevallier, F., Bousquet, P., Logan, M., Peylin, P., and Ramonet, M.: Atmospheric inversions for estimating CO_2 fluxes: methods and perspectives, Climatic Change, 103, 69–92, 2010.

Enting, I. G., Trudinger, C. M., and Francey, R. J.: A synthesis inversion of the concentration and $\delta^{13}C$ of atmospheric CO_2, Tellus B, 47, 35–52, 1995.

Gatti, L. V., Miller, J. B., D'Amelio, M. T. S., Martinewski, A., Basso, L. S., Gloor, M. E., Wofsy, S., and Tans, P.: Vertical profiles of CO_2 above eastern Amazonia suggest a net carbon flux to the atmosphere and balanced biosphere between 2000 and 2009, Tellus B, 62, 581–594, doi:10.1111/j.1600-0889.2010.00484.x, 2010.

Gatti, L. V., Gloor, M., Miller, J. B., Doughty, C. E., Malhi, Y., Domingues, L. G., Basso, L. S., Martinewski, A., Correia, C. S. C., Borges, V. F., Freitas, S., Braz, R., Anderson, L. O., Rocha, H., Grace, J., Phillips, O. L., and Lloyd, J.: Drought sensitivity of Amazonian carbon balance revealed by atmospheric measurements, Nature, 506, 76–80, doi:10.1038/nature12957, 2014.

Gloor, M., Gatti, L., Brienen, R., Feldpausch, T. R., Phillips, O. L., Miller, J., Ometto, J. P., Rocha, H., Baker, T., de Jong, B., Houghton, R. A., Malhi, Y., Aragão, L. E. O. C., Guyot, J.-L., Zhao, K., Jackson, R., Peylin, P., Sitch, S., Poulter, B., Lomas, M., Zaehle, S., Huntingford, C., Levy, P., and Lloyd, J.: The carbon balance of

South America: a review of the status, decadal trends and main determinants, Biogeosciences, 9, 5407–5430, doi:10.5194/bg-9-5407-2012, 2012.

Goulden, M. L., Miller, S. D., da Rocha, H. R., Menton, M. C., de Freitas, H. C., e Silva Figueira, A. M., and de Sousa, C. A. D.: Diel and seasonal patterns of tropical forest CO_2 exchange, Ecol. Appl., 14, 42–54, doi:10.1890/02-6008, 2004.

Grace, J., Malhi, Y., Lloyd, J., McIntyre, J., Miranda, A. C., Meir, P., and Miranda, H. S.: The use of eddy covariance to infer the net carbon dioxide uptake of Brazilian rain forest, Glob. Change Biol., 2, 209–217, doi:10.1111/j.1365-2486.1996.tb00073.x, 1996.

Hourdin, F., Musat, I., Bony, S., Braconnot, P., Codron, F., Dufresne, J.-L., Fairhead, L., Filiberti, M.-A., Friedlingstein, P., Grandpeix, J.-Y., Krinner, G., LeVan, P., Li, Z.-X., and Lott, F.: The LMDZ4 general circulation model: climate performance and sensitivity to parametrized physics with emphasis on tropical convection, Clim. Dynam., 27, 787–813, doi:10.1007/s00382-006-0158-0, 2006.

Huete, A. R., Didan, K., Shimabukuro, Y. E., Ratana, P., Saleska, S. R., Hutyra, L. R., Yang, W., Nemani, R. R., and Myneni, R.: Amazon rainforests green-up with sunlight in dry season, Geophys. Res. Lett., 33, L06405, doi:10.1029/2005GL025583, 2006.

INPE: Projeto de Monitoramento do Desmatamento na Amazônia Legal por Satélite (PRODES), available at: http://www.obt.inpe.br/prodes/index.php (last access: 4 May 2014), 2011.

Jung, M., Reichstein, M., Margolis, H. A., Cescatti, A., Richardson, A. D., Arain, M. A., Arneth, A., Bernhofer, C., Bonal, D., Chen, J., Gianelle, D., Gobron, N., Kiely, G., Kutsch, W., Lasslop, G., Law, B. E., Lindroth, A., Merbold, L., Montagnani, L., Moors, E. J., Papale, D., Sottocornola, M., Vaccari, F., and Williams, C.: Global patterns of land–atmosphere fluxes of carbon dioxide, latent heat, and sensible heat derived from eddy covariance, satellite, and meteorological observations, J. Geophys. Res., 116, G00J07, doi:10.1029/2010JG001566, 2011.

Kirchhoff, V. W. J. H., Aires, C. B., and Alvala, P. C.: An experiment to determine atmospheric CO concentrations of tropical South Atlantic air samples, Quart. J. Roy. Meteor. Soc., 129, 1891–1902, doi:doi10.1256/qj.02.142, 2003.

Krinner, G., Viovy, N., de Noblet-Ducoudré, N., Ogée, J., Polcher, J., Friedlingstein, P., Ciais, P., Sitch, S., and Prentice, I. C.: A dynamic global vegetation model for studies of the coupled atmosphere–biosphere system, Global Biogeochem. Cy., 19, GB1015, doi:10.1029/2003GB002199, 2005.

Law, R. M., Steele, L. P., Krummel, P. B., and Zahorowski, W.: Synoptic variations in atmospheric CO_2 at Cape Grim: a model intercomparison, Tellus B, 62, 810–820, doi:10.1111/j.1600-0889.2010.00470.x, 2010.

Lewis, S. L., Brando, P. M., Phillips, O. L., van der Heijden, G. M. F., and Nepstad, D.: The 2010 Amazon drought, Science, 331, p. 554, doi:10.1126/science.1200807, 2011.

Lloyd, J., Kolle, O., Fritsch, H., de Freitas, S. R., Silva Dias, M. A. F., Artaxo, P., Nobre, A. D., de Araújo, A. C., Kruijt, B., Sogacheva, L., Fisch, G., Thielmann, A., Kuhn, U., and Andreae, M. O.: An airborne regional carbon balance for Central Amazonia, Biogeosciences, 4, 759–768, doi:10.5194/bg-4-759-2007, 2007.

Maignan, F., Bréon, F.-M., Chevallier, F., Viovy, N., Ciais, P., Garrec, C., Trules, J., and Mancip, M.: Evaluation of a Global Vegetation Model using time series of satellite vegetation indices, Geosci. Model Dev., 4, 1103–1114, doi:10.5194/gmd-4-1103-2011, 2011.

Malhi, Y., Roberts, J. T., Betts, R. A., Killeen, T. J., Li, W., and Nobre, C. A.: Climate change, deforestation, and the fate of the Amazon, Science, 319, 169–172, 2008.

Malhi, Y., Aragão, L. E. O. C., Galbraith, D., Huntingford, C., Fisher, R., Zelazowski, P., Sitch, S., McSweeney, C., and Meir, P.: Exploring the likelihood and mechanism of a climate-change-induced dieback of the Amazon rainforest, P. Natl. Acad. Sci. USA, 106, 20610–20615, doi:10.1073/pnas.0804619106, 2009.

Marengo, J. A., Ronchail, J., Baez, J., and Alves, L.: State of the climate in 2009, in: The Climate of Tropical South America East of the Andes, vol. 91, American Meteorological Society, Boston, MA, USA, S148–S150, 2010.

Miller, S. D., Goulden, M. L., Menton, M. C., da Rocha, H. R., de Freitas, H. C., Figueira, A. M. E. S., and Dias de Sousa, C. A.: Biometric and micrometeorological measurements of tropical forest carbon balance, Ecol. Appl., 14, 114–126, doi:10.1890/02-6005, 2004.

Moreira, D. S., Freitas, S. R., Bonatti, J. P., Mercado, L. M., Rosário, N. M. É., Longo, K. M., Miller, J. B., Gloor, M., and Gatti, L. V.: Coupling between the JULES land-surface scheme and the CCATT-BRAMS atmospheric chemistry model (JULES-CCATT-BRAMS1.0): applications to numerical weather forecasting and the CO_2 budget in South America, Geosci. Model Dev., 6, 1243–1259, doi:10.5194/gmd-6-1243-2013, 2013.

Morton, D. C., Nagol, J., Carabajal, C. C., Rosette, J., Palace, M., Cook, B. D., Vermote, E. F., Harding, D. J., and North, P. R. J.: Amazon forests maintain consistent canopy structure and greenness during the dry season, Nature, 506, 7487, doi:10.1038/nature13006, 2014.

Negrón-Juárez, R. I., Chambers, J. Q., Guimaraes, G., Zeng, H., Raupp, C. F. M., Marra, D. M., Ribeiro, G. H. P. M., Saatchi, S. S., Nelson, B. W., and Higuchi, N.: Widespread Amazon forest tree mortality from a single cross-basin squall line event, Geophys. Res. Lett., 37, L16701, doi:10.1029/2010GL043733, 2010.

Olivier, J. and Berdowski, J.: Global emissions sources and sinks, in: The Climate System, A. A. Balkema Publishers/Swets & Zeitlinger Publishers, Lisse, 33–78, 2001.

Ometto, J. P. H. B., Nobre, A. D., Rocha, H. R., Artaxo, P., and Martinelli, L. A.: Amazonia and the modern carbon cycle: lessons learned, Oecologia, 143, 483–500, 2005.

Parazoo, N. C., Denning, A. S., Kawa, S. R., Corbin, K. D., Lokupitiya, R. S., and Baker, I. T.: Mechanisms for synoptic variations of atmospheric CO_2 in North America, South America and Europe, Atmos. Chem. Phys., 8, 7239–7254, doi:10.5194/acp-8-7239-2008, 2008.

Parazoo, N. C., Bowman, K., Frankenberg, C., Lee, J.-E., Fisher, J. B., Worden, J., Jones, D. B. A., Berry, J., Collatz, G. J., Baker, I. T., Jung, M., Liu, J., Osterman, G., O'Dell, C., Sparks, A., Butz, A., Guerlet, S., Yoshida, Y., Chen, H., and Gerbig, C.: Interpreting seasonal changes in the carbon balance of southern Amazonia using measurements of XCO_2 and chlorophyll fluorescence from GOSAT, Geophys. Res. Lett., 40, 2829–2833, doi:10.1002/grl.50452, 2013.

Peylin, P., Baker, D., Sarmiento, J., Ciais, P., and Bousquet, P.: Influence of transport uncertainty on annual mean and seasonal inversions of atmospheric CO_2 data, J. Geophys. Res., 107, 4385, doi:10.1029/2001JD000857, 2002.

Peylin, P., Law, R. M., Gurney, K. R., Chevallier, F., Jacobson, A. R., Maki, T., Niwa, Y., Patra, P. K., Peters, W., Rayner, P. J., Rödenbeck, C., van der Laan-Luijkx, I. T., and Zhang, X.: Global atmospheric carbon budget: results from an ensemble of atmospheric CO_2 inversions, Biogeosciences, 10, 6699–6720, doi:10.5194/bg-10-6699-2013, 2013.

Phillips, O. L., Aragão, L. E. O. C., Lewis, S. L., Fisher, J. B., Lloyd, J., López-González, G., Malhi, Y., Monteagudo, A., Peacock, J., Quesada, C. A., van der Heijden, G., Almeida, S., Amaral, I., Arroyo, L., Aymard, G., Baker, T. R., Bánki, O., Blanc, L., Bonal, D., Brando, P., Chave, J., de Oliveira, A. C. A., Cardozo, N. D., Czimczik, C. I., Feldpausch, T. R., Freitas, M. A., Gloor, E., Higuchi, N., Jiménez, E., Lloyd, G., Meir, P., Mendoza, C., Morel, A., Neill, D. A., Nepstad, D., Patiño, S., Peñuela, M. C., Prieto, A., Ramírez, F., Schwarz, M., Silva, J., Silveira, M., Thomas, A. S., Steege, H. T., Stropp, J., Vásquez, R., Zelazowski, P., Dávila, E. A., Andelman, S., Andrade, A., Chao, K.-J., Erwin, T., Di Fiore, A. C. E. H., Keeling, H., Killeen, T. J., Laurance, W. F., Cruz, A. P., Pitman, N. C. A., Vargas, P. N., Ramírez-Angulo, H., Rudas, A., Salamão, R., Silva, N., Terborgh, J., and Torres-Lezama, A.: Drought sensitivity of the Amazon rainforest, Science, 323, 1344–1347, 2009.

Piao, S., Sitch, S., Ciais, P., Friedlingstein, P., Peylin, P., Wang, X., Ahlström, A., Anav, A., Canadell, J. G., Cong, N., Huntingford, C., Jung, M., Levis, S., Levy, P. E., Li, J., Lin, X., Lomas, M. R., Lu, M., Luo, Y., Ma, Y., Myneni, R. B., Poulter, B., Sun, Z., Wang, T., Viovy, N., Zaehle, S., and Zeng, N.: Evaluation of terrestrial carbon cycle models for their response to climate variability and to CO_2 trends, Glob. Chang. Biol., 19, 2117–2132,doi:10.1111/gcb.12187, 2013.

Poulter, B., Heyder, U., and Cramer, W.: Modeling the sensitivity of the seasonal cycle of GPP to dynamic LAI and soil depths in tropical rainforests, Ecosystems, 12, 517–533, doi:10.1007/s10021-009-9238-4, 2009.

Randerson, J. T., van der Werf, G. R., Giglio, L., Collatz, G. J., and Kasibhatla, P. S.: Global Fire Emissions Database, Version 2.1. Data set from Oak Ridge National Laboratory Distributed Active Archive Center, Oak Ridge, Tennessee, USA, doi:10.3334/ORNLDAAC/849, available at: http://daac.ornl.gov/ (last access: 9 September 2013), 2007.

Saatchi, S., Asefi-Najafabady, S., Malhi, Y., Aragão, L. E. O. C., Anderson, L. O., Myneni, R. B., and Nemani, R.: Persistent effects of a severe drought on Amazonian forest canopy, P. Natl. Acad. Sci. USA, 110, 565–570, 2012.

Saleska, S. R., Miller, S. D., Matross, D. M., Goulden, M. L., Wofsy, S. C., da Rocha, H. R., de Camargo, P. B., Crill, P., Daube, B. C., de Freitas, H. C., Hutyra, L., Keller, M., Kirchhoff, V., Menton, M., Munger, J. W., Pyle, E. H., Rice, A. H., and Silva, H.: Carbon in Amazon forests: unexpected seasonal fluxes and disturbance-induced losses, Science, 302, 1554–1557, 2003.

Saleska, S. R., Didan, K., Huete, A. R., and da Rocha, H. R.: Amazon forests green-up during 2005 drought, Science, 318, 612–612, 2007.

Samanta, A., Ganguly, S., Hashimoto, H., Devadiga, S., Vermote, E., Knyazikhin, Y., Nemani, R. R., and Myneni, R. B.: Amazon forests did not green-up during the 2005 drought, Geophys. Res. Lett., 37, L05401, doi:10.1029/2009GL042154, 2010.

Samanta, A., Ganguly, S., Vermote, E., Nemani, R. R., and Myneni, R. B.: Interpretation of variations in MODIS-measured greenness levels of Amazon forests during 2000 to, Environ. Res. Lett., 7, 024018, doi:10.1088/1748-9326/7/2/024018, 2012.

Takahashi, T., Sutherland, S. C., Wanninkhof, R., Sweeney, C., Feely, R. A., Chipman, D. W., Hales, B., Friederich, G., Chavez, F., Sabine, C., Watson, A., Bakker, D. C., Schuster, U., Metzl, N., Yoshikawa-Inoue, H., Ishii, M., Midorikawa, T., Nojiri, Y., Körtzinger, A., Steinhoff, T., Hoppema, M., Olafsson, J., Arnarson, T. S., Tilbrook, B., Johannessen, T., Olsen, A., Bellerby, R., Wong, C., Delille, B., Bates, N., and de Baar, H. J.: Climatological mean and decadal change in surface ocean pCO_2, and net sea–air CO_2 flux over the global oceans, Deep-Sea Res. Pt. II, 56, 554–577, 2009.

Tarantola, A.: Inverse Problem Theory and Methods for Model Parameter Estimation, Society for Industrial and Applied Mathematics, Philadelphia, 2005.

Verbeeck, H., Peylin, P., Bacour, C., Bonal, D., Steppe, K., and Ciais, P.: Seasonal patterns of CO_2 fluxes in Amazon forests: fusion of eddy covariance data and the ORCHIDEE model, J. Geophys. Res., 116, G02018, doi:10.1029/2010JG001544, 2011.

von Randow, C., Manzi, A. O., Kruijt, B., de Oliveira, P. J., Zanchi, F. B., Silva, R. L., Hodnett, M. G., Gash, J. H. C., Elbers, J. A., Waterloo, M. J., Cardoso, F. L., and Kabat, P.: Comparative measurements and seasonal variations in energy and carbon exchange over forest and pasture in south west Amazonia, Theor. Appl. Climatol., 78, 5–26, doi:10.1007/s00704-004-0041-z, 2004.

Wang, W., Ciais, P., Nemani, R. R., Canadell, J. G., Piao, S., Sitch, S., White, M. A., Hashimoto, H., Milesi, C., and Myneni, R. B.: Variations in atmospheric CO_2 growth rates coupled with tropical temperature, P. Natl. Acad. Sci. USA, 110, 13061–13066, doi:10.1073/pnas.1219683110, 2013.

Xu, L., Samanta, A., Costa, M. H., Ganguly, S., Nemani, R. R., and Myneni, R. B.: Widespread decline in greenness of Amazonian vegetation due to the 2010 drought, Geophys. Res. Lett., 38, L07402, doi:10.1029/2011GL046824, 2011.

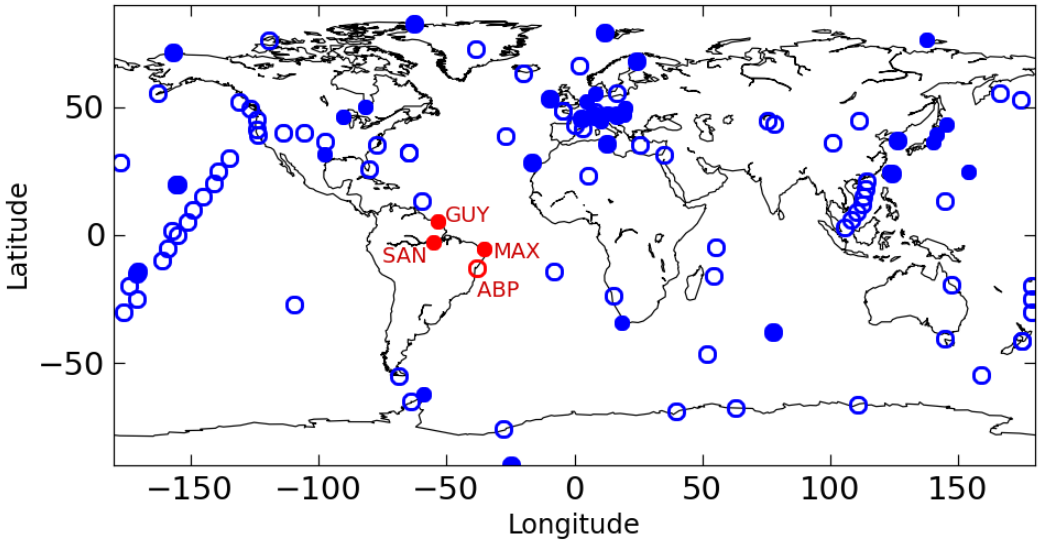

Figure 1. Location of the surface stations used in this study. Blue: surface stations used in MACCv10.1, red: surface stations in South America added to the previous setup of MACCv10.1. Filled circles: stations with continuous measurements, open circles: sites with discrete air sampling.

Station	Period of data availability for this study									Principal investigator
	2002	2003	2004	2005	2006	2007	2008	2009	2010	
Arembepe (ABP)										E. Dlugokencky ESRL, NOAA, Boulder, Colorado, USA
Guyaflux (GUY)										D. Bonal, INRA, Nancy, France and B. Burban, INRA, Kourou, French Guiana
Maxaranguape (MAX)										B. Munger Harvard University, Cambridge, Massachusetts, USA
Santarém (SAN)										S. Wofsy Harvard University, Cambridge, Massachusetts, USA

Figure 2. List of surface stations over South America added to the previous setup in MACCv10.1.

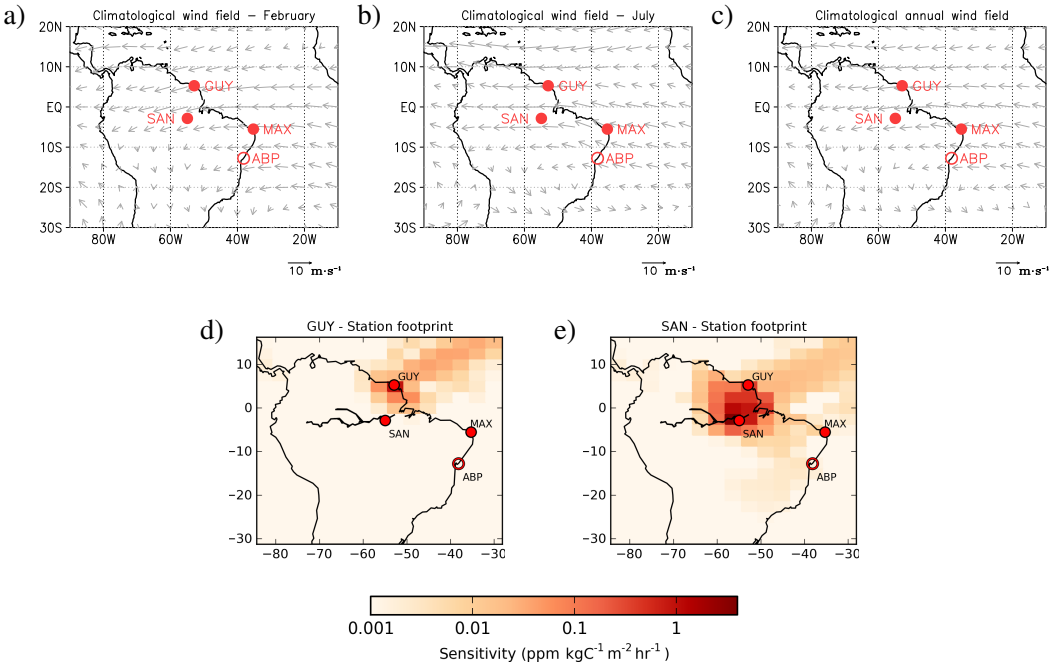

Figure 3. Top: Location of assimilated surface stations in South America and climatological wind speed/direction for February **(a)**, July **(b)**, and annual mean **(c)**, averaged over 1981–2010 between the surface and a level of 600 hPa (Source: NCEP/NCAR Reanalysis). Sensitivity of surface atmospheric CO_2 mole fractions measured on 20 February 2009 at 10:00 UTC, at Guyaflux (7:00 LT) (d) and Santarém (6:00 LT) (e), to a constant increment of surface fluxes during the two days prior to the measurement. Sensitivity values are expressed in log-scale. Open circles: sites with discrete air samplings. Filled circles: measurements taken with continuous analysers.

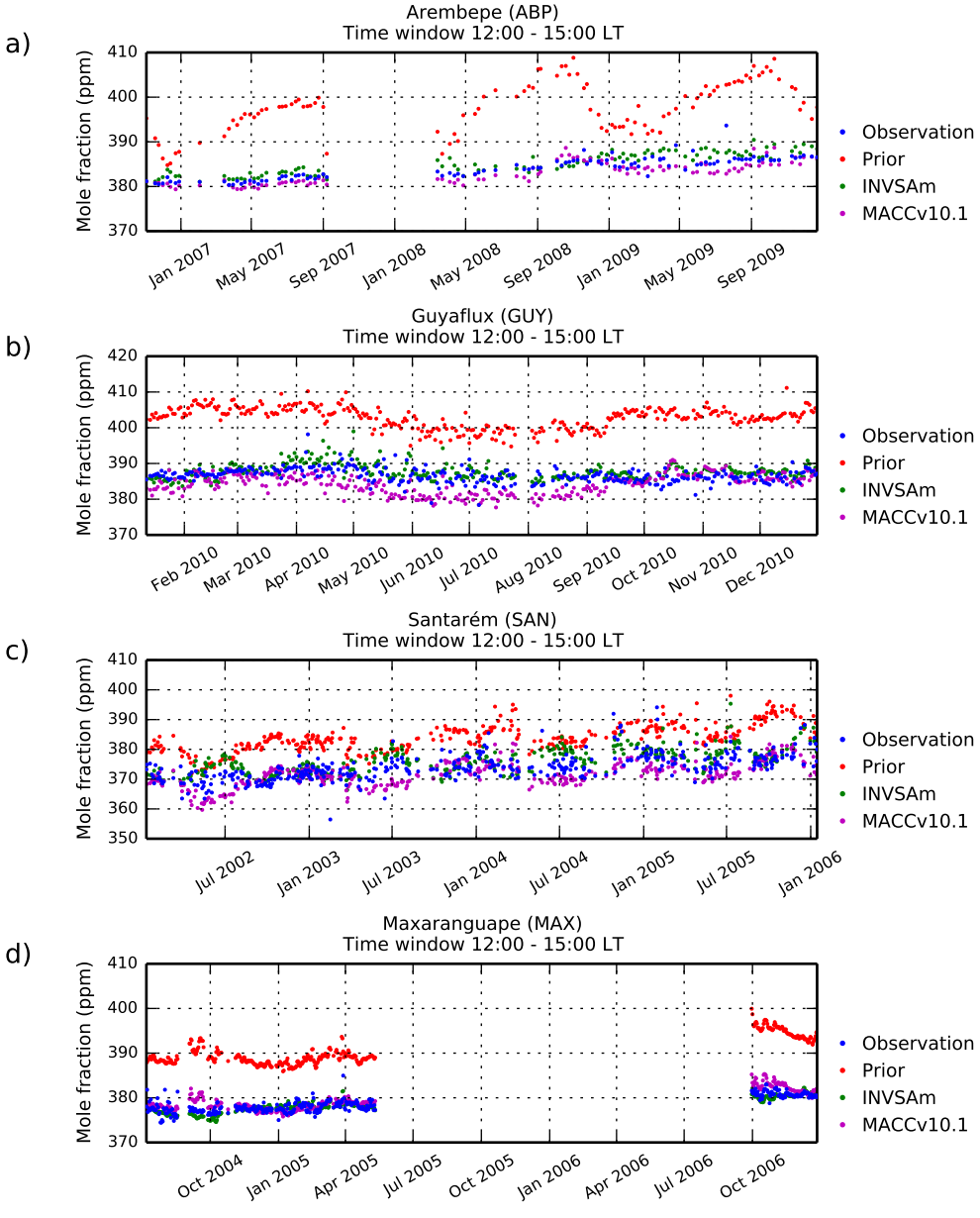

Figure 4. Comparison of assimilated CO_2 observations (blue) and corresponding simulated mole fractions using prior fluxes (red), INVSAm (green) and MACCv10.1 (purple). Measurements were collected at Arembepe **(a)**, Guyaflux **(b)**, Santarém **(c)** and Maxaranguape **(d)**. Data shown here correspond to daily average mole fractions between 12:00 and 15:00 local time (LT), when wind speed $> 2\,\mathrm{m\,s^{-1}}$. Note that the time scale differs between plots.

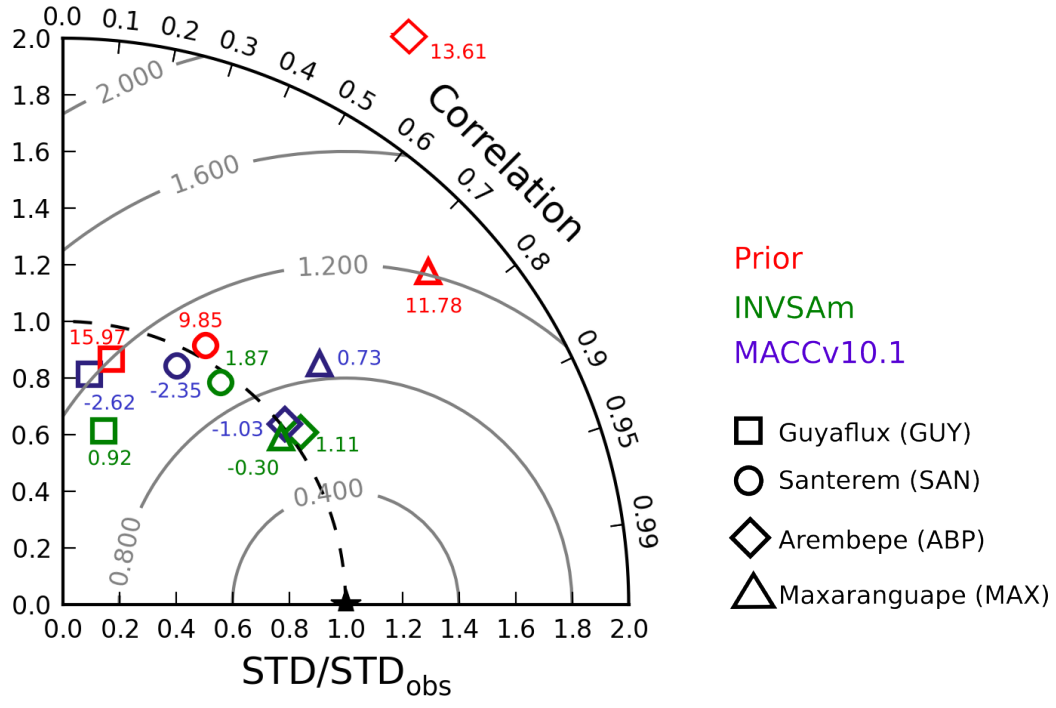

Figure 5. Taylor diagram of the statistics of misfits between observations and simulated CO_2 mole fractions between 12:00 and 15:00 LT at Guyaflux (square), Santarém (circle), Arembepe (diamond) and Maxaranguape (triangle), when wind speed $> 2\,\mathrm{m\,s^{-1}}$, using prior fluxes (red), INVSAm (green) and MACCv10.1 (purple). Radial distance from the origin: ratio of SD of simulated mole fractions and SD of the observations. Angle measured from the y axis: coefficient of correlation. Numbers next to the symbols: bias (in ppm). Gray circles: SD of the misfits (in ppm).

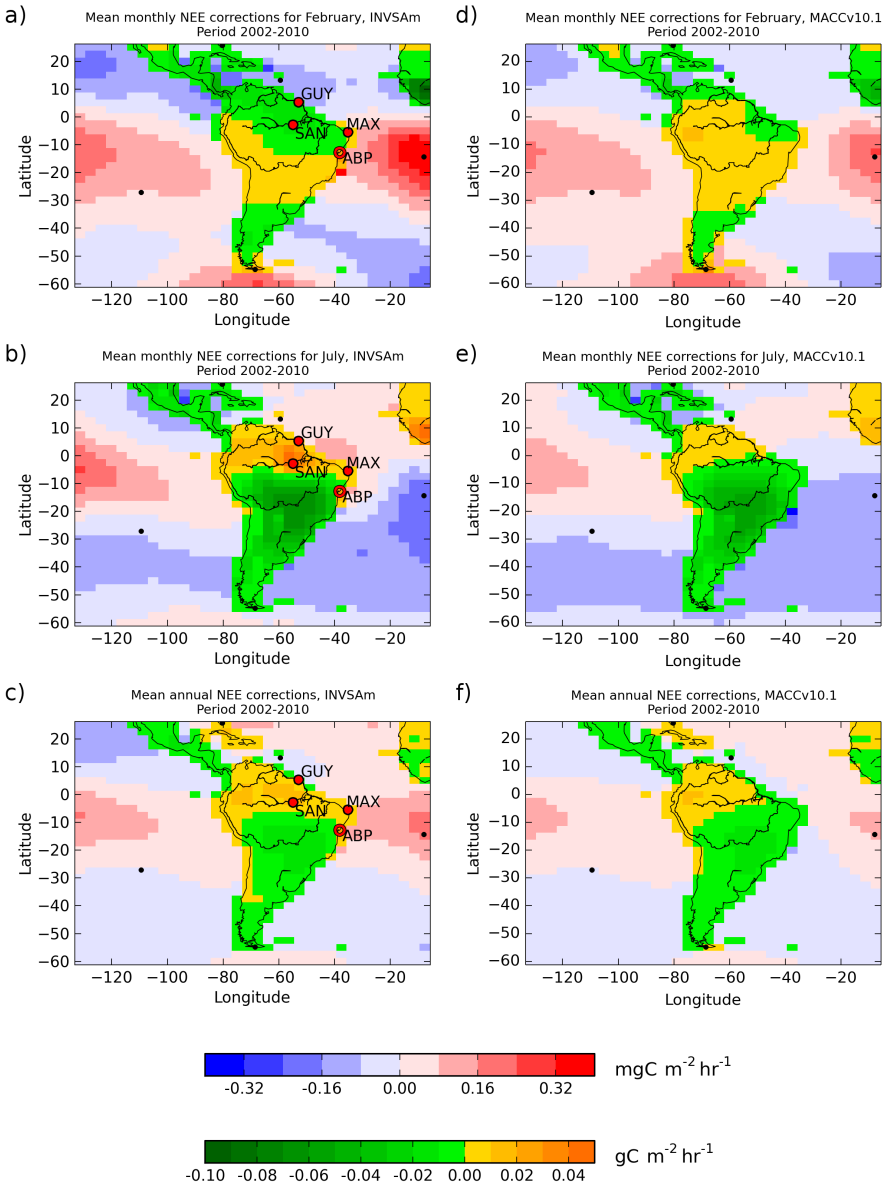

Figure 6. Spatial distribution of 2002–2010 mean flux corrections at the transport model resolution ($3.75^\circ \times 2.50^\circ$) to ORCHIDEE from INVSAm (left) and MACCv10.1 (right) over an area larger than TSA region: mean for February **(a,d)**, July **(b,e)**, and mean over the full period 2002–2010 **(c,f)**. Flux increments over land and ocean are represented with two distinct colour scales and units: green–yellow for land, in $\mathrm{gC\,m^{-2}\,hr^{-1}}$; blue–red for ocean, in $\mathrm{mgC\,m^{-2}\,hr^{-1}}$. Red symbols: surface stations in South America added to the previous setup of MACCv10.1, where filled circles indicate locations of sites with continuous measurements; open circles indicate locations of sites with discrete air sampling. Black symbols: surface stations used in MACCv10.1.

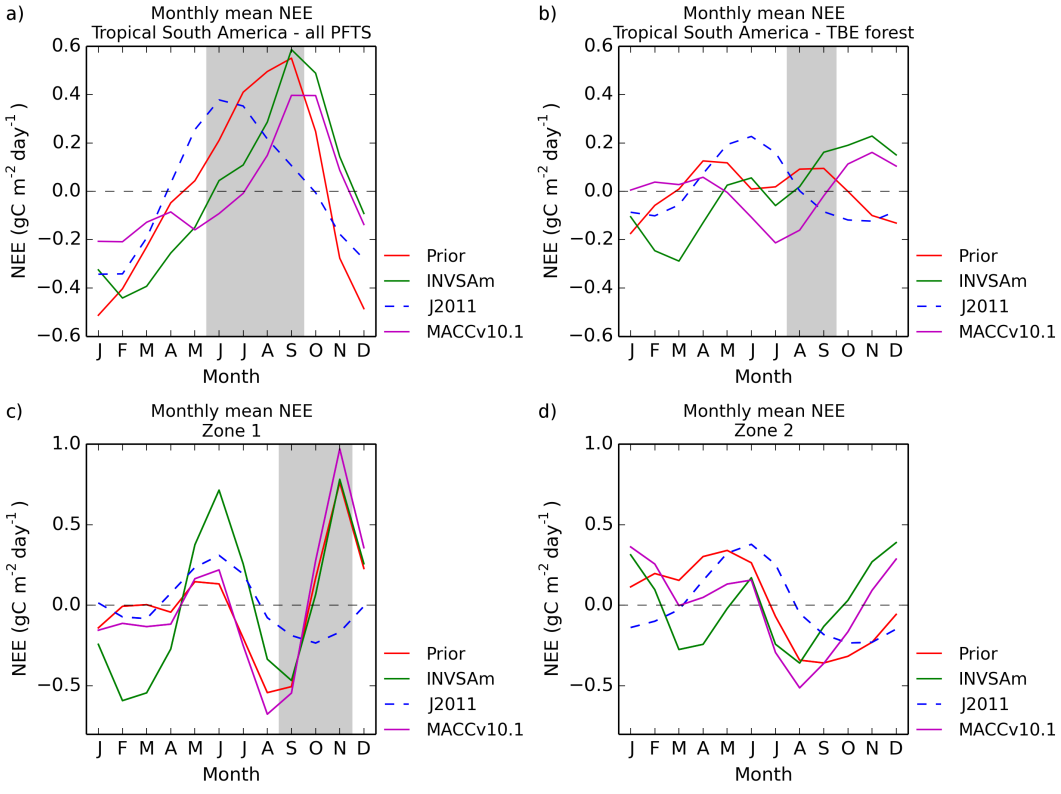

Figure 7. Monthly mean NEE anomaly integrated over **(a)** the TSA region and **(b)** over pixels dominated by TBE forests in ORCHIDEE for 2002–2010. The shaded areas denote dry seasons, defined as months with precipitation $< 100\,\mathrm{mm}$, based on monthly totals from TRMM data over 2002–2010. Estimates from prior fluxes (red), INVSAm (green), MACCv10.1 (purple) and J2011 (dashed blue). **(c–d)** Monthly mean NEE integrated over the zones 1 **(c)** and 2 **(d)** that are defined in Fig. 8.

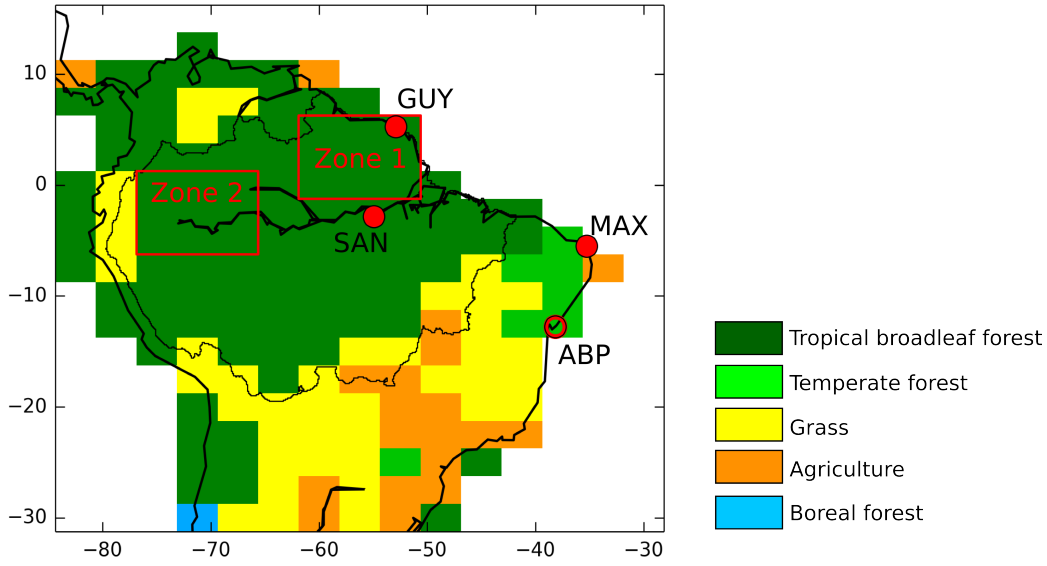

Figure 8. Dominant PFTs for each transport model grid cell (i.e. $3.75^\circ \times 2.50^\circ$) according to the ORCHIDEE vegetation map over the TSA region. Open circles show location of sites with discrete air sampling; filled circles show location of sites with continuous measurements. Zones 1 and 2 indicate areas for which the NEE is presented in Figs. 7c and d, respectively.

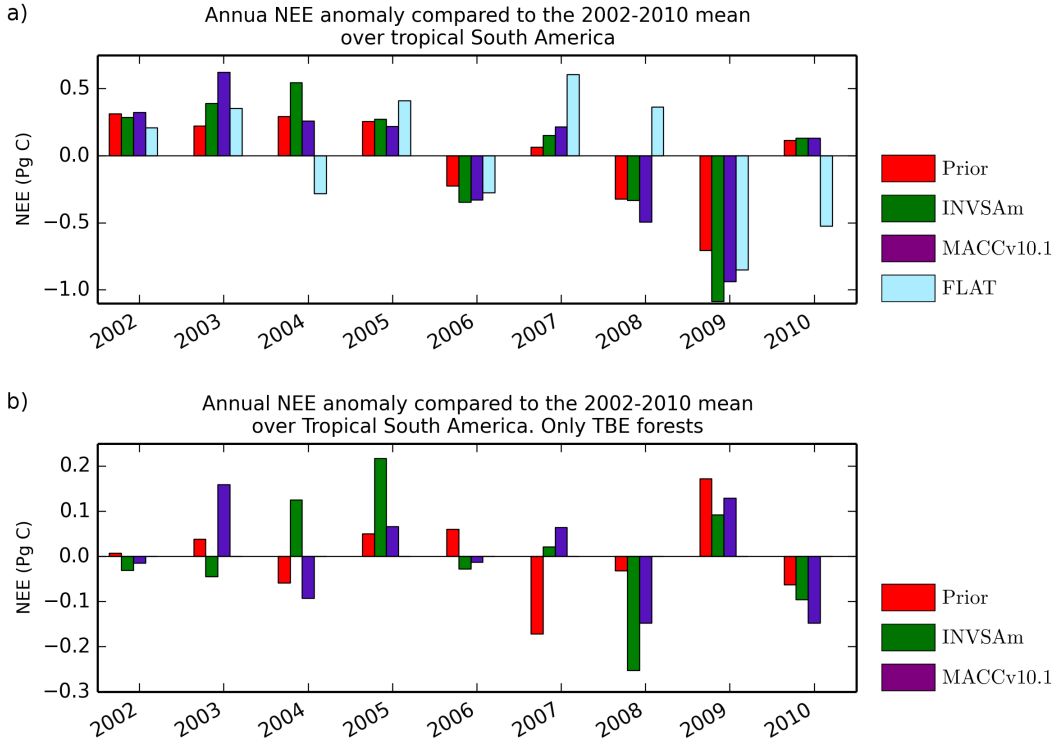

Figure 9. **(a)** Annual NEE anomaly compared to the mean of 2002–2010; estimates for the TSA region. **(b)** Annual NEE anomaly compared to the mean of 2002–2010; estimates for the area dominated by TBE forests.

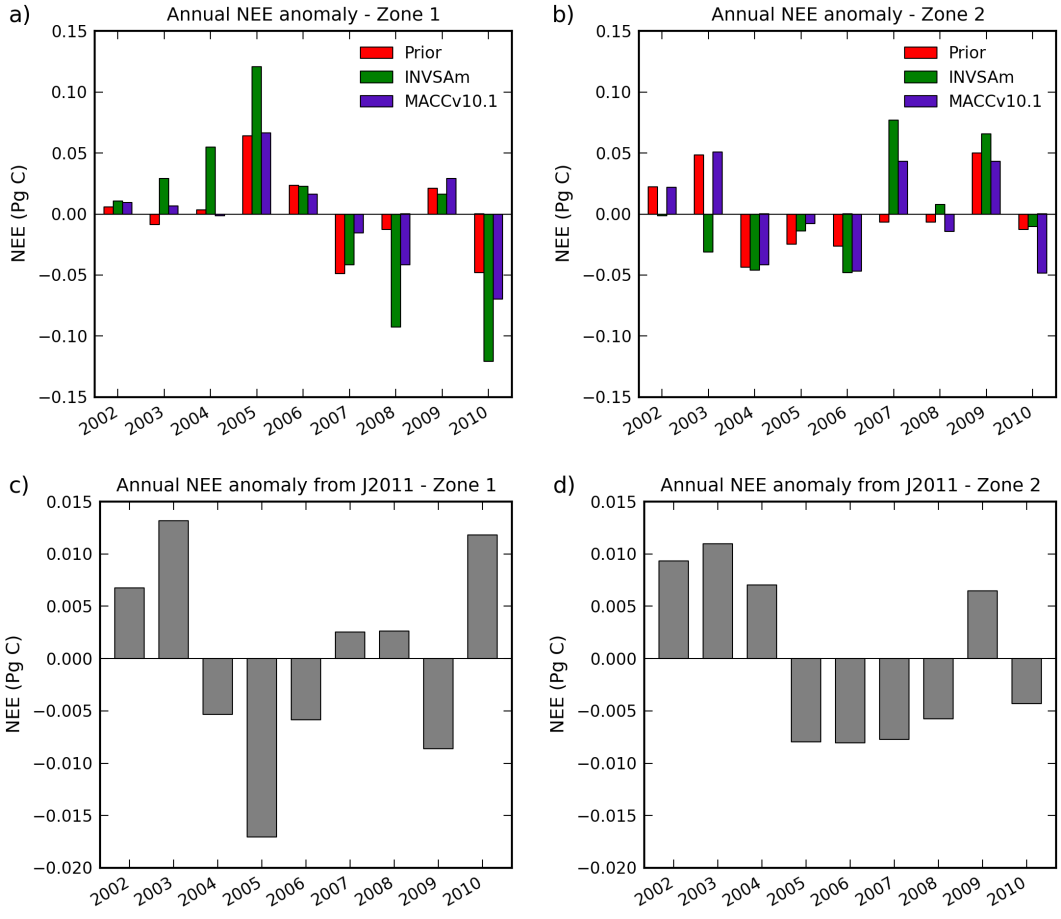

Figure 10. Annual NEE anomaly compared to the 2002–2010 mean for Zone 1 **(a, c)** and Zone 2 **(b, d)** as defined in Fig. 8. Estimates from prior fluxes (red), INVSAm (green), MACCv10.1 (purple), and J2011 (gray).